scientific reports

Check for updates

OPEN

Investigation of piezoelectric printing devices for oil-free and on-demand picolitre monodisperse droplet generation

Zhenlin Wu[1], Shaoshuai Han[1], Hu Meng[1], Di Lian[1], Tongfei Wu[1], Wenjie Chu[1], He Li[1], Mengting Ning[1], Bingjie Wang[1], Xijing Gao[1], Shizhao Xu[2], Jun Ren[3]✉ & Xin Yang[4]

Picolitre monodisperse droplet printing technology has important applications in biochemistry, such as accounting for quantitative analysis and single-cell analysis, and can be used for parallel high-throughput analysis of biomarkers and chemicals. However, commonly used droplet generation devices require complex control systems or customised microfluidic chips, making them costly and difficult for researchers to operate. Additionally, generating picolitre monodisperse droplets with microfluidic devices necessitates the introduction of an oil phase to block and separate the liquid. This requirement can reduce the throughput of the target droplets and cause cell contamination, hindering the adoption of this technology. By employing a common 1-mm-diameter capillary in the laboratory in combination with a piezoelectric transducer, we have achieved on-demand picolitre droplet printing of less than 100 pL in an oil-free environment. The device was found to be biocompatible with K562 cells. This approach is less costly, offers greater operational freedom, and is easier to integrate with other downstream assay modules or even handheld cell-printing devices. This study holds great potential for application in areas such as single-cell analysis, cell sampling, and pharmaceutical analysis.

Picolitre monodisperse droplet printing technology has many applications in chemistry and biology, such as nucleic acid determination[1,2], cell culture[3], drug analysis[4] and single cell analysis[5–7], in addition to its potential for use in key components of dispensing machines. Particularly for the controlled printing of picolitre droplets, reagent losses can be significantly reduced, and control of reagent mixing, transfer and interactions can be improved. Currently the most widely used platform for droplet generation is microfluidics, such as cross-flow[8], isotropic flow[9], and flow-focusing[10,11] structures, which offer the advantages of uniform size distribution, tunable droplet composition, high throughput, and downstream analytical integration[12,13]. However, due to the complexity of microfluidic channel processes providing micrometer- or even nanometer-precision for pL droplet generation, and the fact that most microfluidic droplet generation techniques inevitably require the use of oil to provide the conditions for generating continuous droplets[14,15], with the consequences of high system complexity, poor fluidic controllability, and high sample loss. The droplet generation machines that currently exist on the market are expensive not only for the complex instruments, but also for their key core components and single droplet print chips (approximately $30–240 for a disposable print chip or design cartridge)[16] and are poorly integrated with other test steps such as bioanalysis.

In order to generate monodisperse droplet in a cheaper, less time-consuming, and simpler way, researchers have now created a number of methods. Some researchers have used glass capillaries, a common item in biochemistry, to generate microdroplets. For example, Li et al. combined microscope slides with stretched glass capillaries to generate monodisperse multiple emulsions[17].Gu et al. used a 75 μm fused silica capillary to create and manipulate droplets for a single-cell assay[18]. He et al. generated an ultra-wide range (6.77–66 μm) and high throughput (5000 drops/s) of micrometer droplets by high-frequency tapping of a piezoelectric transducer (PZT) into the capillary outlet[19], by which they performed digital PCR with a large dynamic range and multiplexing capability. Although the above mentioned devices are less costly than conventional microfluidic devices, they are

[1]School of Optoelectronic Engineering and Instrumentation Science, Dalian University of Technology, Dalian 116024, China. [2]Dalian Municipal Central Hospital, Central Hospital of Dalian University of Technology, Dalian 116024, China. [3]Liaoning Key Laboratory of Molecular Recognition and Imaging, School of Bioengineering, Dalian University of Technology, Dalian 116024, China. [4]Department of Electrical and Electronics Engineering, School of Engineering, Cardiff University, Cardiff CF10 3AT, UK. ✉email: renjun@dlut.edu.cn

not suitable for rapid adaptation and use by novice researchers due to the licensed capillary size requirements and post-processing needed to generate pico-scale droplets. Other researchers have utilized microelectromechanical systems (MEMS) to generate microdroplets[20–22], demonstrating their ability to consistently and precisely produce droplets. However, the size of the generated droplets tends to be relatively large, typically exceeding 1 nL. Additionally, some methods generate droplets by acoustic resonance, where the droplets are generated from the surface of the liquid upwards without contact with the device itself. Such devices can significantly enhance their biocompatibility, but they also present some drawbacks. It limits operational flexibility, increases the complexity of downstream detection procedures, and poses challenges for integration with other microfluidic modules[23].

In this study, we utilize a commonly used 1 mm diameter capillary in conjunction with a ring PZT to develop a picolitre monodisperse droplet printing technique for on-demand printing in oil-free environments. This approach offers lower costs, increased operational flexibility, and easier integration into other downstream assay modules or even handheld cell printing devices. The current device, comprising a ring PZT combined with a laser-perforated metal steel sheet, forms a bulk acoustic wave device capable of precisely printing liquids in capillary tubes as droplets of less than 100 pL volume. We explore the droplet generation mechanism through multiphysics field simulation and validate the device's robustness and stability through experimental analysis. Furthermore, we investigate the device's excellent biocompatibility by printing human chronic myeloid leukemia cells (K562). Our experiments demonstrate the device's significant potential for application in the fields of cell analysis and single-cell printing.

Results and discussion

This study focuses on providing a simple and fast picolitre droplet printing device that can greatly reduce the research threshold for scholars. With this device, target biological solutions can be effortlessly drawn through capillary microtubules and encapsulated into picolitre microdroplets. This technology can provide the essential technical capabilities for cell printing techniques, enabling their application in downstream biological and chemical analyses. Meanwhile, in combination with other bioanalytical software, the encapsulation effect of homogenized picolitre droplets and the subsequent culture effect can be observed intuitively and effectively, as shown in Fig. 1. And the physical and device diagrams of the droplet printing nozzle are depicted in Fig. S1. As syringe pumps and intricate microfluidic channels were not employed in this study, it can be more easily integrated with biochemical analyses such as digital PCR and single-cell analysis, thereby reducing the complexity of sample pre-treatment.

As shown in Fig. 2a, the deformation process within a micropore during a control signal cycle is depicted. The PZT generates alternating tensile and compressive forces on the metal sheet while manipulating the alternating signal. These forces transmit through the metal sheet to the center of the aggregation, causing periodic vibration of the inner wall of the micropore. Consequently, this vibration affects the volume of the micropore, the liquid within it, and the air environment, leading to pressure changes conducive to the generation of liquid droplets. Thus, by ensuring a periodic variation of the control signal, the vibrations of the PZT can be coupled into the steel sheet to induce droplet generation in the micropores. This process allows for selective droplet printing by controlling the on–off switch of the radio frequency signal. The magnified image highlights a pore with a diameter of 30 μm. As depicted in Fig. S4, the micropore was processed using a high-energy pulsed laser, followed by acid washing and ultrasonic cleaning to smooth the edges, thereby facilitating a smoother device printing process. Ensuring the uniformity of device preparation and processing is critical for its large-scale application.

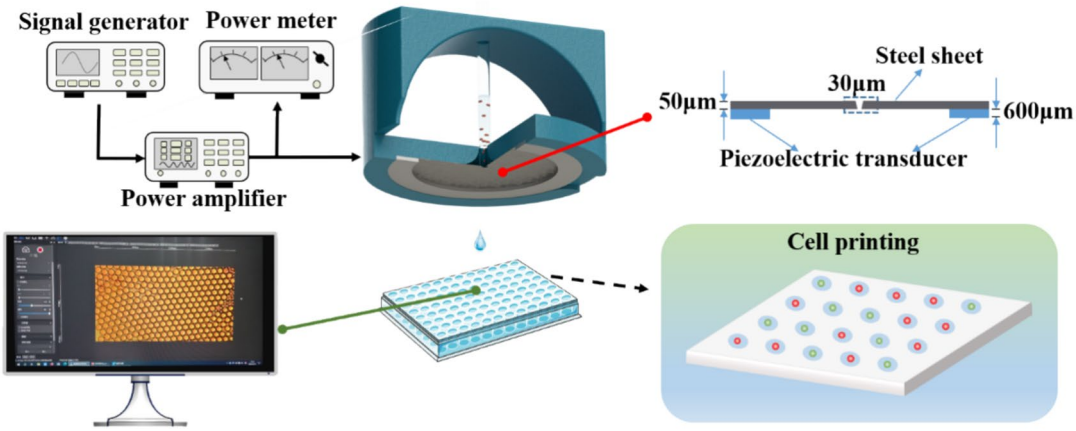

Figure 1. Schematic diagram of the experimental link for the PZT-based cell printing device. This picolitre monodisperse droplet printing technology provides an easy-to-use technical solution for cell printing. A cutaway view of the print nozzle is shown in the centre of the diagram, and a 1 mm diameter capillary tube draws up the solution and is placed directly onto the PZT, which will be free of adhesion, ensuring that the capillary tube is aligned with the micropore. The device consists of a dimensional view of the core components: a ring PZT with a thickness of 600 μm, a metal sheet with a thickness of 50 μm, and a micropore with a diameter of 30 μm. The picolitre monodisperse droplet printing device can be used in bioengineering applications such as cell printing.

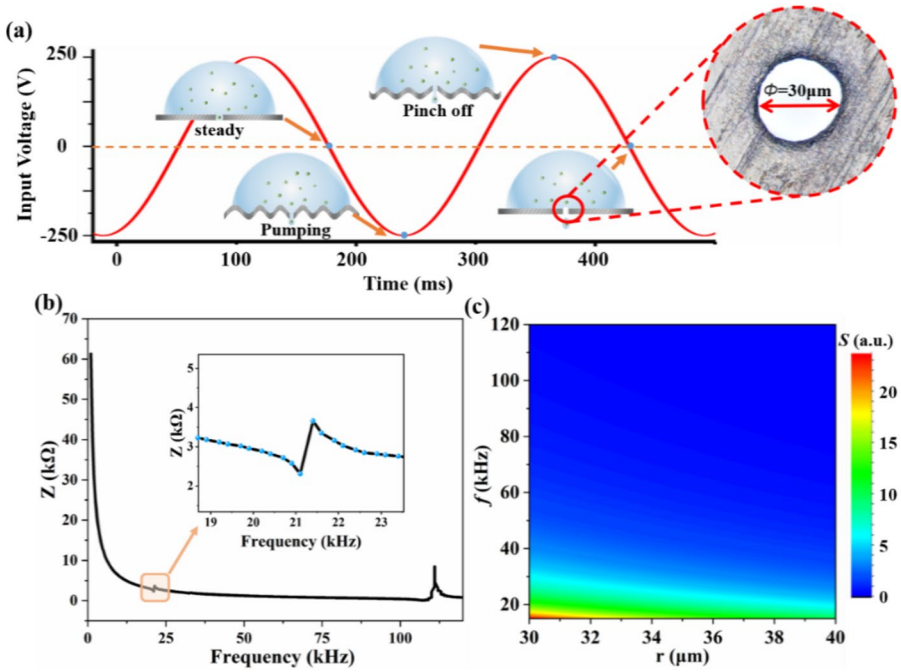

Figure 2. PZT based picolitre monodisperse droplet printing principle. (**a**) Throughout one cycle of input RF signal, the droplet printing device transitions through steady, pumping, and pinch off to ultimately realize droplet generation. (**b**) By analyzing the Bode plot obtained from the impedance analysis of the PZT droplet printing device, it is possible to determine the resonance frequency of the PZT with a local peak. (**c**) As the diameter of the micropores in the metal sheet and the input frequency change, the value of the dimensionless surface tension parameter *S* also changes, and the critical conditions for droplet generation can be judged based on the distribution.

The droplet printing device was assessed using an impedance analyzer, revealing resonant frequencies peaking around 21 kHz and 112 kHz, as illustrated in Fig. 2b. At the resonant frequency of the PZT, the amplitude at the center of the micropores increases, accelerating the liquid on the micropores. When the inertial force exceeds the surface tension holding the droplets on the micropores, the liquid then pinches off and produces droplets.

The generation of droplets is influenced by the pore size of micropores, the signal frequency, and the type of fluid. For instance, taking deionized water (DI water) as an example, we introduce the dimensionless surface tension parameter *S* is introduced here[24].

$$S = \frac{2\sigma}{\rho r^3 f^2} \tag{1}$$

where σ is the surface tension of the liquid, ρ is the density of the liquid, r is the radius of the micropores, and f is the frequency. S should be equal to or greater than 1 for droplets to detach from the liquid–air interface. Otherwise, the amplitude of the ripples would be too small to cause droplet detachment from the liquid surface. The surface tension of DI water used in the experiments was 0.072 N/m. In Fig. 2c, the effect of different pore internal diameters and input frequencies on the S parameter is illustrated. It can be observed that with an increase in frequency, the dimensionless surface tension parameter decreases significantly. The resonant frequency of 112 kHz at PZT, besides being the resonance frequency of the PZT, is less than 1. Therefore, under this control condition, the vibration frequency of the micropores is too fast to provide sufficient amplitude for droplet generation. This aligns with the experimental procedure, where the PZT only produces a sharp chirp at signal frequencies near 112 kHz, but does not result in droplet production. Hence, subsequent droplet-related experiments were conducted at signal frequencies near 20 kHz.

Finite element simulations of the PZT-based upgraded droplet printing technique were conducted using COMSOL Multiphysics 6.1. Figure 3a illustrates the pressure distribution of the device. It is evident that the vibration induced by the PZT under the alternating signal propagates along the metal sheet towards the center. A high-pressure region is formed around the central pore due to the convergence of vibrations. Figure 3b presents a multiphysics simulation integrating hydrodynamics, illustrating the pressure distribution of the liquid in the capillary microtube above the metal sheet. The vibration amplitude of the metal sheet is on the order of micrometers, and the propagation pattern aligns with Fig. 3a. When the acoustic wave interacts with the droplet, the acoustic surface wave is coupled upward into the droplet, creating a high-pressure region around the liquid column. And the particles around the micropores will move from the high-pressure region to the low-pressure region due to the pressure distribution, which provides the possibility of cell printing[25,26]. We also analysed the

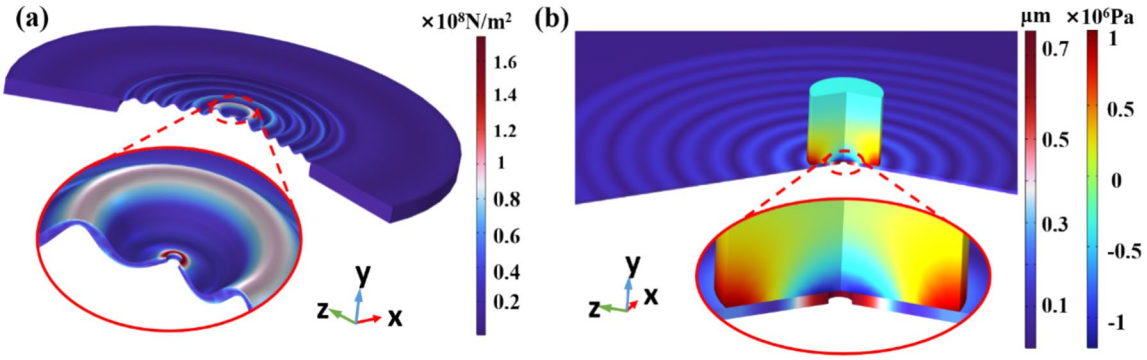

Figure 3. Multi-physics field simulation of a droplet generation device based on PZTs. (**a**) Plot of the pressure distribution of a metal sheet at a frequency of 16 kHz. (**b**) Vibration amplitude distribution of a metal sheet at a frequency of 16 kHz, also including the internal pressure distribution of a 1 mm diameter liquid column.

thermodynamic distribution of the devices, as shown in Fig. S3. The pressure field distribution occupies the main factor in the cause of monodisperse droplet generation.

With a defined range of resonant frequencies, it's essential to ensure sufficient vibration amplitude to provide ample energy for droplet generation. The voltage of the control signal determines the amplitude of vibration of the PZT, thus necessitating an analysis of the impact of control signal voltage a nd frequency on droplet printing. A significant challenge with single droplet devices is the inevitable production of satellite droplets, which can adversely affect the accuracy of subsequent quantitative analyses such as digital PCR. Hence, it's crucial to explore control conditions that can stabilize the generation of single droplets in single droplet printing devices. As illustrated in Fig. 4a, the single-droplet generation conditions of this device indicate that single droplets are consistently produced within a signal voltage range of 200 V to 221 V and a control signal frequency range of 12 kHz to 20 kHz, with no satellite droplets observed. These findings were statistically analyzed to underscore the device's robustness to variations in control signal frequency, thereby enhancing its usability for operators. Figure 4b depicts the variation in input voltage by adjusting the input signal frequency to 16 kHz. The findings reveal that voltage within the range of 270 V produces a single droplet, with the droplet volume changing according to the voltage. However, exceeding a certain voltage threshold leads to excessive vibration amplitude in the center micropore, resulting in the formation of satellite droplets and uncontrollable droplet volume. We have found through experiments that if the nozzle becomes clogged, it can be cleared using two methods. Firstly, wiping the nozzle with alcohol effectively removes blockages. Alternatively, changing the trigger signal to continuous wave mode causes the nozzle to vibrate at a high frequency, which helps dislodge and clean the obstruction by continuously splashing liquid.

In bioengineering applications, digital PCR, for example, requires the rapid division of micro samples into quantitative micro units. In addition to the small volume requirement, the speed of droplet generation is also a key parameter. In this study, the number of droplets generated per second is controlled by controlling the Burst Period (BP) of the signal generator. Figure 4c shows that the droplet diameter increases from 20 μm to 30 μm when the Burst Period is varied from 500 to 5 ms. The experiment was investigated by building a two-dimensional kinematic platform, as shown in Fig. S2.The reason for this phenomenon is that when the Burst Period is smaller, the vibration amplitude of the micropores varies more strongly due to inertia, and thus the droplet volume is larger. It can be concluded that the volume of individual droplets decreases with increasing pulse period. As shown in Fig. 4d, the volume of individual droplets stabilises in the volumetric region when the pulse period decreases to 400 ms. This phenomenon is due to the physical properties of the micropores. Droplets with too small a volume will not be able to detach from the liquid in the micropore due to surface tension. And similarly, as the pulse period increases, the velocity of the droplet's motion decreases with inertial circularity.

To explore the potential applications of picolitre monodisperse droplet generation technique across various fields, ensuring droplet homogeneity and compatibility with biological particles is imperative. Figure 5 depicts the homogeneity analysis of the device across different droplet diameters. It is evident that the dispersion of small-diameter droplets is minimal compared to large-diameter ones, remaining predominantly within the target droplet diameter range of ± 4 μm. Compared to oil-phase droplet generation[27,28], the dynamic range of droplet generation in the device described in this study is influenced by the size of the micropores. However, this trade-off can significantly reduce the complexity of the operation and the construction costs for researchers, while maintaining microdroplets with good homogeneity and stability. To expand the device's applicability in manipulating biological particles such as cells, it is necessary to investigate its biocompatibility of the device. Figure 6 illustrates the impact of the device on the biological activity and viability of K562 cells manipulated with the device. As depicted in Fig. 6a, there is a decreasing trend in cell activity with increasing voltage. This phenomenon is due to the fact that the high voltage signal increases the vibration amplitude of the micropores and reduces the activity of the otherwise fragile part of the cells, but this is within tolerance during application. We also performed experimental analyses on HEK293 cells, as shown in Fig. S5, and the results continue to indicate that the device has good biocompatibility.The effect of the device on cell activity was investigated by showing the propagation of printed K562 cells after 72 h of continuous culture, as shown in Fig. 6b. It can be seen that the printed cells are clearly outlined and proliferate normally after 72 h of incubation.

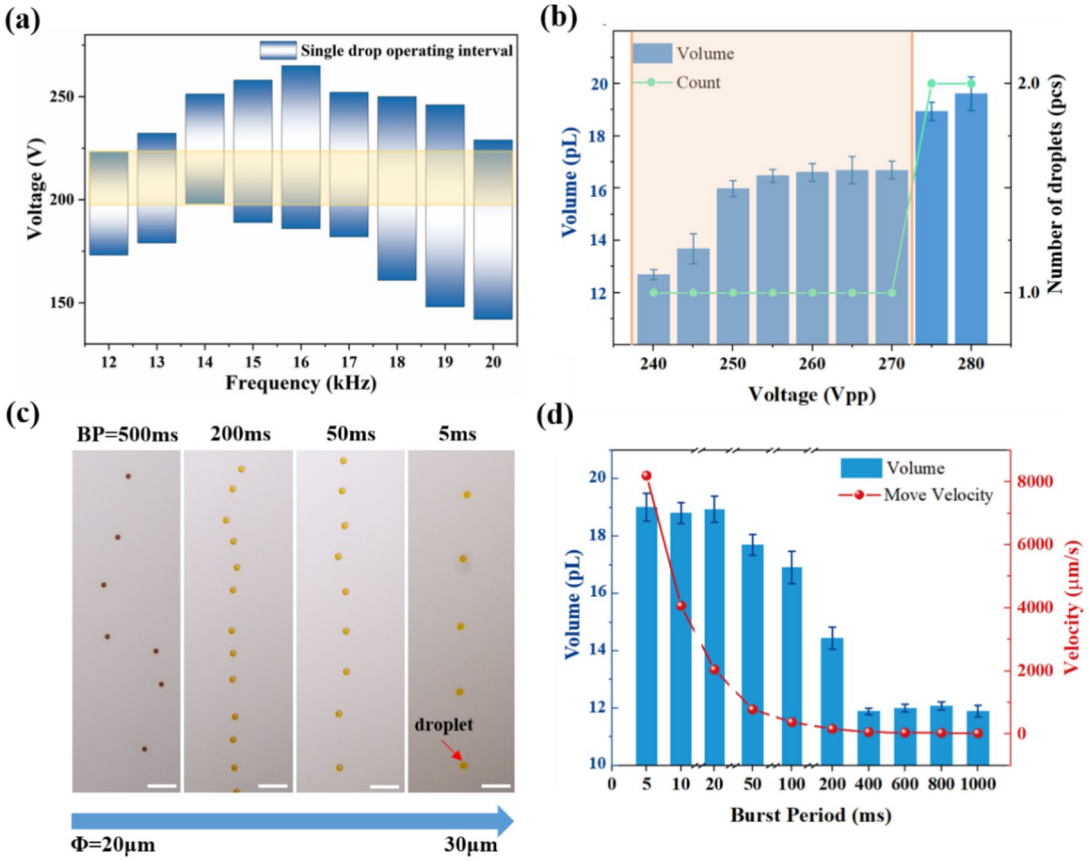

Figure 4. Quantitative experiments of picolitre monodisperse droplet printing. (**a**) Frequency and voltage distribution of the input signal that can realize the effect of single droplet printing, where the yellow area indicates that the device has good robustness to the input signal that realizes single droplet printing. (**b**) Under the trigger of a single pulse cycle signal, the volume of droplets printed by the device changes as the voltage of the control signal changes, due to changes in the amplitude of the micropores. When a certain threshold is reached, the amplitude of the micropores is too large resulting in the production of too many droplets per unit cycle of the signal (comet droplets). (**c**) The droplet diameter of the signal varies at different pulse periods (500 ms-5 ms), and the number of droplets generated per unit time can be controlled according to this parameter. (**d**) Distribution curve of droplet generation volume and motion velocity with control signal pulse period. Scale bar is 100 μm.

Conclusions

Picolitre monodisperse droplets are pivotal across chemistry, biology, medicine, and materials science. Despite various documented technical solutions, generating these droplets has remained complex and costly, posing barriers for researchers with limited expertise and budgets. In this study, we leverage a standard 1-mm-diameter laboratory capillary with a PZT to achieve on-demand printing of droplets smaller than 100 pL in an oil-free environment. This approach reduces costs, enhances operational flexibility, and facilitates integration into downstream assay modules or handheld cell-printing devices. The device demonstrates robust signal manipulation capabilities without requiring complex multi-fluid handling like syringe pumps for oil injection, thereby lowering operational barriers for researchers. Uniform droplet sizes and high biocompatibility make it a user-friendly tool for critical biochemistry tasks such as cell printing and digital PCR.

Methods

Experimental sample preparation

The picolitre droplet printing device used in the experiment consists of a circular metallic steel sheet and a PZT ring. The diameter and thickness of the metallic steel sheet are 16 mm and 0.05 mm, respectively, and the inner diameter, outer diameter, and thickness of the ceramic sheet are 12 mm, 16 mm, and 0.6 mm, respectively, and their dimensions are shown in Fig. 1. They were bonded by glue to ensure that the acoustic surface waves of the PZT could be well coupled and propagated with the metal steel sheet. The metallic steel sheet is punched several times with a high-energy pulsed laser to a diameter of about 80 μm, followed by an acid-washing operation to ensure that the holes are as smooth as possible. Another structure in the device is a capillary tube of 1 mm diameter, which is commonly used in laboratories.

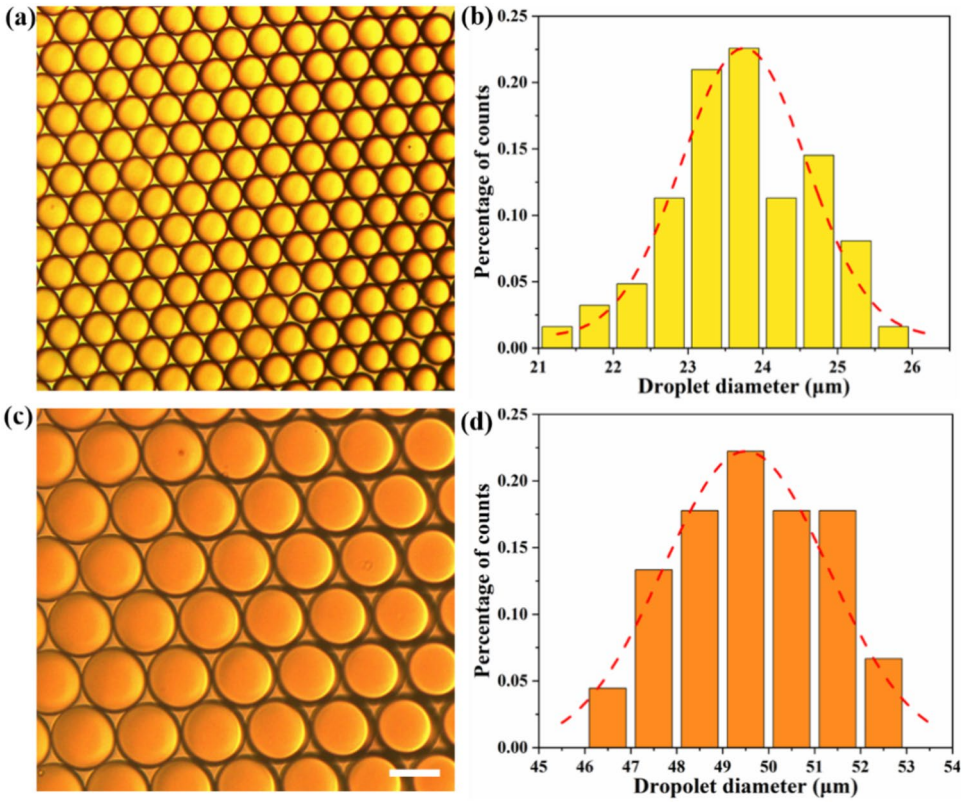

Figure 5. Results and Statistics of the generated microdroplets. (**a**) Optical bright-field micrographs of droplets around 25 μm in diameter are produced. (**b**) Produces a particle size uniformity distribution of microdroplets with a diameter of about 25 μm. (**c**) Produces an optical bright-field micrograph of a droplet with a diameter of about 50 μm. (**d**) Produces a particle size uniformity distribution of microdroplets with a diameter of about 50 μm. The scale bar is 50 μm. The above experiments used droplet-specific oils (2% surfactant in HFE 7500) to prevent intermiscibility of the printed droplets, and picolitre-scale droplets were printed directly into oils packed in microtiter plates during the experiments.

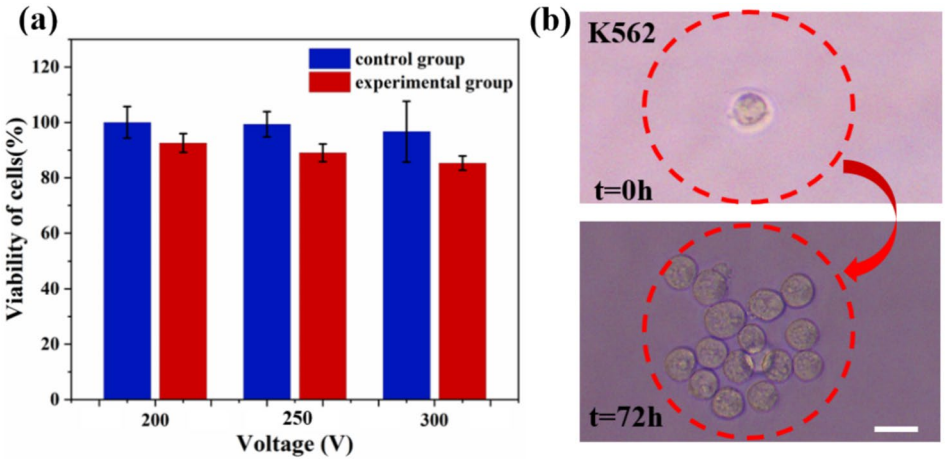

Figure 6. Effect of picolitre droplet printing technique on cell viability and activity. (**a**) The effect on the viability of printed K562 cells with different input signal voltages. (**b**) The printed k562 cells still have good propagation ability. The scale bar is 20 μm. The experiment was carried out in a bio-specific fume hood as a way to ensure sterility and prevent contamination.

Fabrication of picolitre monodisperse droplets printing device based on PZT ring

The single-droplet printing in the first stage of the experiment used deionized water with dye, which was prepared by mixing red dye (Neutral red PH0523 PHYGENE) and DI water in the ratio of 1:10. The biological solution for cell printing was human chronic myelogenous leukemia cells (K562), which was prepared by preparing Roswell Park Memorial Institute (RPMI-1640) complete medium containing 10% fetal bovine serum (FBS) as well as some essential amino acids and vitamins. Cells were taken after 24 h of culture after resuscitation and passaged. Trypsin was added to the cells rinsed with PBS and left in the incubator for about 2 min, then the cell mass was broken down into individual dispersed cells and suspended in the culture medium. Add complete medium and centrifuge at 1500 rpm for 8 min. The cell precipitate was taken and mixed with 1 mL of medium and diluted to prepare the initial experimental solution.

Determination of cellular activity

The study of the effect of the droplet printing device on cell activity is of great importance for downstream analysis and. In this study, we mainly use CCK8 to detect cell activity to analyze the effect of the device on cell activity under different voltages. The specific steps are firstly, five groups of blank group, control group and experimental group were set up in 96-well plates. Using a cell suspension with a cell concentration of 5×10^6 cells/mL, after passing through the droplet printing device, a 20 μL sample was taken and counted using a cell counter (Vi-CELL BLU Cell Viability Analyzer,USA) to confirm the number of cells passing through the device. The experimental cell suspension was then inoculated into a 96-well plate with a corresponding control group, ensuring that the amount of liquid in each well was 100 μL. 5000 cells were inoculated in each well of the experimental and control groups. In each well, 10 μL of CCK8 reagent was added according to the ratio, and the absorbance was measured at 450 nm using a Microplate reader (TECAN Infinite 200 PRO, Switzerland), and the results of cell activity in the control and experimental groups were calculated. The above experiments were repeated for 5 groups at 200 V, 250 V and 300 V respectively.

Data availability

Data is provided within the manuscript or supplementary information files.

Received: 12 April 2024; Accepted: 16 July 2024
Published online: 23 July 2024

References

1. Kumaresan, P., Yang, C. J., Cronier, S. A., Blazej, R. G. & Mathies, R. A. High-throughput single copy DNA amplification and cell analysis in engineered nanoliter droplets. *Anal. Chem.* **80**, 3522–3529 (2008).
2. Jin, S. H. *et al.* Monitoring of chromosome dynamics of single yeast cells in a microfluidic platform with aperture cell traps. *Lab Chip* **16**, 1358–1365 (2016).
3. Siltanen, C. A. *et al.* An oil-free picodrop bioassay platform for synthetic biology. *Sci. Rep.* **8**, 7913 (2018).
4. Wang, Y. & Wang, J. Mixed hydrogel bead-based tumor spheroid formation and anticancer drug testing. *Analyst* https://doi.org/10.1039/C4AN00015C (2014).
5. Bintu, B. *et al.* Super-resolution chromatin tracing reveals domains and cooperative interactions in single cells. *Science* **362**, eaau1783 (2018).
6. Jin, S. *et al.* Inference and analysis of cell-cell communication using Cell Chat. *Nat. Commun.* **12**, 1088 (2021).
7. Giladi, A. *et al.* Dissecting cellular crosstalk by sequencing physically interacting cells. *Nat. Biotechnol.* **38**, 629–637 (2020).
8. Zhu, P. & Wang, L. Passive and active droplet generation with microfluidics: A review. *Lab Chip* **17**, 34–75 (2017).
9. Baroud, C. N., Gallaire, F. & Dangla, R. Dynamics of microfluidic droplets. *Lab Chip* **10**, 2032 (2010).
10. Bardin, D., Kendall, M. R., Dayton, P. A. & Lee, A. P. Parallel generation of uniform fine droplets at hundreds of kilohertz in a flow-focusing module. *Biomicrofluidics* **7**, 034112 (2013).
11. Hatch, A. C., Patel, A., Beer, N. R. & Lee, A. P. Passive droplet sorting using viscoelastic flow focusing. *Lab Chip* **13**, 1308 (2013).
12. Korczyk, P. M. *et al.* Accounting for corner flow unifies the understanding of droplet formation in microfluidic channels. *Nat. Commun.* **10**, 2528 (2019).
13. Dangla, R., Kayi, S. C. & Baroud, C. N. Droplet microfluidics driven by gradients of confinement. *Proc. Natl. Acad. Sci. U. S. A.* **110**, 853–858 (2013).
14. Li, J. *et al.* Formation of polarized, functional artificial cells from compartmentalized droplet networks and nanomaterials, using one-step, dual-material 3D-printed microfluidics. *Adv. Sci.* **7**, 1901719 (2020).
15. Jiang, C.-Y. *et al.* High-throughput single-cell cultivation on microfluidic streak plates. *Appl. Environ. Microbiol.* **82**, 2210–2218 (2016).
16. Baker, M. Digital PCR hits its stride. *Nat. Methods* **9**, 541–544 (2012).
17. Li, E. Q., Zhang, J. M. & Thoroddsen, S. T. Simple and inexpensive microfluidic devices for the generation of monodisperse multiple emulsions. *J. Micromech. Microeng.* **24**, 015019 (2014).
18. Gu, S.-Q. *et al.* Multifunctional picoliter droplet manipulation platform and its application in single cell analysis. *Anal. Chem.* **83**, 7570–7576 (2011).
19. He, Z. *et al.* A portable droplet generation system for ultra-wide dynamic range digital PCR based on a vibrating sharp-tip capillary. *Biosensors Bioelectron,* **191**, 113458 (2021).
20. Zhou, Y. *et al.* Pinch-off droplet generator using microscale gigahertz acoustics. *Lab Chip* **23**, 4860–4867 (2023).
21. Chen, K. *et al.* A digital acoustofluidic device for on-demand and oil-free droplet generation. *Nanotechnology* **30**, 084001 (2019).
22. Dumas, S., Richerd, M., Serra, M. & Descroix, S. Magnetic microtweezers: A tool for high-throughput bioseparation in sub-nanoliter droplets. *Adv Mater. Technol.* **8**, 2200747 (2023).
23. Schulz, M. *et al.* Versatile tool for droplet generation in standard reaction tubes by centrifugal step emulsification. *Molecules* **25**, 1914 (2020).
24. Perçin, G. & Khuri-Yakub, B. T. Piezoelectric droplet ejector for ink-jet printing of fluids and solid particles. *Rev. Sci. Instr.* **74**, 1120–1127 (2003).
25. Jian, X. *et al.* Single-cell microliter-droplet screening system (MISS Cell): An integrated platform for automated high-throughput microbial monoclonal cultivation and picking. *Biotech. Bioeng.* **120**, 778–792 (2023).
26. Zhou, X., Wu, H., Wen, H. & Zheng, B. Advances in single-cell printing. *Micromachines* **13**, 80 (2022).

27. Wang, X. *et al.* Droplet volume modulation based on multi-waveform superposition for drop-on-demand material jetting. *Addit. Manuf.* **79**, 103940 (2024).
28. Zhang, P. & Abate, A. R. High-definition single-cell printing: Cell-by-cell fabrication of biological structures. *Adv. Mater.* **32**, 2005346 (2020).

Acknowledgements

This work is supported by "Dalian Life and Health Planning Project"(2022ZXYG22) and "Fundamental Research Funds for the Central Universities"(2022ZXYG22).

Author contributions

Z.W., J.R. and X,Y. proposed the conceptualization and methodology; Z.W., S.H. and J.R. analyzed the data, reviewed and modified the manuscript; S.H., D.L. and T.W performed the experiments. S.H. and Z.W. wrote the original draft preparation; H.M. and W.C. carried out the simulations; H.L. edited and revised the article; M.N., B.W. and X.G. contributed investigation; S.X. conducted biological experiments.

Competing interests

The authors declare no competing interests.

Additional information

Supplementary Information The online version contains supplementary material available at https://doi.org/10.1038/s41598-024-67849-2.

Correspondence and requests for materials should be addressed to J.R.

Reprints and permissions information is available at www.nature.com/reprints.

Publisher's note Springer Nature remains neutral with regard to jurisdictional claims in published maps and institutional affiliations.